J. Fluid Mech. (2006), *vol.* 549, *pp.* 81–98.
doi:10.1017/S0022112005007056 Printed in the United Kingdom

The absolute instability of an inviscid compound jet

By ANUJ CHAUHAN[1]†, CHARLES MALDARELLI[1]‡, DEMETRIOS T. PAPAGEORGIOU[2] AND DAVID S. RUMSCHITZKI[1]‡

[1]The Levich Institute and Department of Chemical Engineering, City College of CUNY, New York, NY 10031, USA

[2]Department of Mathematics, Center for Applied Mathematics and Statistics, New Jersey Institute of Technology, University Heights, Newark, NJ 07102, USA

(Received 1 November 2002 and in revised form 5 July 2005)

This paper examines the emergence of the absolute instability from convectively unstable states of an inviscid compound jet. A compound jet is composed of a cylindrical jet of one fluid surrounded by a concentric annulus of a second, immiscible fluid. For all jet velocities v, there are two convectively unstable modes. As in the single-fluid jet, the compound jet becomes absolutely unstable below a critical dimensionless velocity or Weber number $V(:=\sqrt{v^2\rho_1 R_1/\sigma_1}$ where ρ_1, R_1 and σ_1 are the core density, radius and core–annular interfacial tension), which is a function of the annular/core ratios of densities β, surface tensions γ and radii a. At $V=0$, the absolutely unstable modes and growth recover the fastest growing temporal waves. We focus specifically on the effect of γ at $a=2$ and $\beta=1$ and find that when the outer tension is significantly less than the inner ($0.1<\gamma<0.3$), the critical Weber number V_{crit} decreases with γ, whereas for higher ratios ($0.3<\gamma<3$) it increases. The values (1.2–2.3) of V_{crit} for the compound jet include the parameter-independent critical value of 1.77 for the single jet. Therefore, increasing the outer tension can access the absolute instability at higher dimensional velocities than for a single jet with the same radius and density as the core and a surface tension equal to the compound jet's liquid–liquid tension. We argue that this potentially facilitates distinguishing experimentally between absolute and convective instabilities because higher velocities and surface tension ratios higher than 1 extend the breakup length of the convective instability. In addition, for $0.3<\gamma<1.16$, the wavelength for the absolute instability is roughly half that of the fastest growing convectively unstable wave. Thus choosing γ in this range exaggerates its distinction from the convective instability and further aids the potential observation of absolute instability.

1. Introduction

A liquid jet is unstable to axisymmetric interfacial disturbances owing to destabilizing capillary forces. The linear stability of a base state consisting of a doubly infinite ($z\to\pm\infty$, z is along the thread axis) circular, inviscid, liquid thread

† Present address: Room 237 Chemical Engineering PO Box 116005, University of Florida, Gainesville, FL 32611-6005, USA.

‡ Authors to whom correspondence should be addressed.

with tension σ, uniform radius a and density ρ was first studied by Rayleigh (1879). Rayleigh analysed the *temporal* instability of this base state by imposing, at $t=0$, an interfacial disturbance with Fourier wavenumbers k and n in the z- and θ-directions, respectively. He determined the evolution of this initial disturbance using normal modes ($e^{i(kz+n\theta)+s(k,n)t}$, $s(k,n)=s_r+is_i$ complex). Rayleigh established that only axisymmetric ($n=0$) waves with lengths ($2\pi/k$) larger than the undisturbed thread circumference ($2\pi a$) grow in time ($s_r(k,n=0)>0$), and that there is a maximum in the growth rate at a wavenumber $k_m \cong 0.696/a$. The disturbances grow without travelling, i.e. $s_i(k,n=0)=0$. This temporal stability of the static thread was reconsidered for the case in which the thread fluid is viscous (Chandrasekhar 1961), and when it is surrounded by a second, immiscible viscous liquid (Tomotika 1935). Since capillarity drives the instability, the range of unstable wavelengths remains the same when viscous effects are included, but growth rates are reduced and maximally growing waves are shifted to longer wavelengths.

The temporal linear stability of static threads finds application in predicting the collapse of liquid bridges, particularly in microgravity contexts where fluid tethers and bridges arise naturally, and in polymer processing of thin-walled moulds in terrestrial applications where the high viscosity of the polymer permits free-standing annular threads as the configuration sets. However in most applications a jet issues from a nozzle and breaks into drops downstream. In this case disturbances continually imposed at the nozzle tip (either intentionally through periodic oscillations, or through tip imperfections) grow by the destabilizing action of capillarity as they are convected downstream, until they cause the jet to break up into drops. Drop breakup from jets is important in the technological processes of atomization, ink jet printing (Sweet 1964), fuel injection, particle sorting (Hertzberg, Sweet & Herzberg 1976) and polymer fibre spinning, where in the last case it is desirable to arrange for reduced growth rates so that the jets can polymerize before breakup.

To be more applicable to the breakup of a jet into drops, one might modify the temporal analysis of the static thread base state by applying it in a frame that is translating with dimensional velocity v. For the static thread base state, unstable waves grow without travelling; for a uniformly translating jet base state it is easy to see that the growing disturbances simply convect with the velocity v ($s_i(k)=-ikv$) and grow at the same rate ($s_r(k)$). Based on this analysis, one could conclude that the spatial growth of disintegrating jets is $e^{(s_r(k)/v)z}$, where z is the axial distance from the nozzle tip. However, as first noted by Keller, Rubinow & Tu (1973), the fact that the disturbances are continually imposed on the jet should be accounted for in the stability analysis. They suggested a base state in which the jet is modelled as a circular (doubly) infinite jet moving with uniform velocity, and where interfacial disturbances are imposed locally in space (at $z=0$, for example) and periodically in time with Fourier frequency modes ω. For an inviscid jet and axisymmetric disturbances, Keller *et al.* determined the spatial growth for the harmonic response ($e^{ik(\omega)z+i\omega t}$; $k(\omega)$ complex, $k_i<0$ for spatial growth) as a function of the Weber number ($V=\sqrt{v^2\rho a/\sigma}$). Keller *et al.* demonstrated that for $V^2>3.15$ and dimensionless frequencies or Strouhal numbers ($\omega a/v$) between zero and approximately one (the exact cutoff being a function of V), the localized periodic disturbances grow axially. Thus the spatial analysis allows the calculation of stable and unstable frequencies. For frequencies in the unstable range, one can predict the drop size and distance to breakup (assuming the linear theory is valid up to breakup; see the experimental verification discussed below) since the drops which are formed then have a size which scales as $1/k_r(\omega)$ and the distance downstream to breakup is of order $1/k_i(\omega)$. For

asymptotically large V, they show that $1/k_r(\omega)$ and $1/k_i(\omega)$ tend to v/ω and $v/s_r(k_r)$, respectively; that is, the jet forgets the nozzle.

For $V^2 < 3.15$, a change in form of $k_i(\omega)$ was observed. Leib & Goldstein (1986*b*) demonstrated that below this value of the Weber number, growth in time as well as space occurs, due to a pinch singularity, i.e. a merging of two lower order poles, of the dispersion equation. As a result, one says that the jet is *absolutely* unstable with its harmonic response augmented by a temporal growth at a characteristic k^a (i.e $\exp(\mathrm{i}k^a z + s^a t)$, $s_r^a > 0$) and with both upstream and downstream travelling waves. The spatial growth rate $k_i(\omega)$ is then discontinuous; only part of Keller *et al.*'s branch is valid before the solution jumps to a second branch. Further studies (Leib & Goldstein 1986*a*) examined the effect of fluid viscosity, and demonstrated that the critical Weber number (above which the instability is convective and below which it is absolute) decreases with decreasing Reynolds number ($Re = \rho v a/\mu$). Lin & Lian (1989) demonstrated that for a viscous jet (at fixed Re) surrounded by an inviscid gas, the critical Weber number increases as the density of the surrounding phase increases.

A large body of experiments studying the breakup of jets into drops has been undertaken, usually with a sinusoidal periodic disturbance of frequency ω applied at the nozzle tip (see particularly Chaudhary & Maxworthy 1980; Donnelly & Glaberson 1966; Goedde & Yuen 1970; Pimbley 1976; Rutland & Jameson 1970; Taub 1976 and the review monograph by Yarin 1993). These studies, usually carried out at sufficiently high Weber numbers so that the flow is convectively unstable, are consistent with Keller *et al.*'s (1973) limiting result for $V \to \infty$. The temporal rate s_r in these experiments is the inviscid result since for water, typically the fluid of choice, surface tension forces dominate over viscous forces. Although the breakup process is clearly nonlinear, the surprising reach of the linear theory when a single harmonic is applied is usually attributed to the fact that the influence of additional harmonics generated through nonlinear effects usually arises only very near the break-off point. Vihinen, Honohan & Lin (1997) created a single-fluid jet instability in a microgravity environment (a drop tower) and obtained images of the breakup both above and below the critical value (based on the nozzle radius) for absolute instability. Beyond the threshold they observed what resembles upstream as well as downstream travelling waves and interpreted this as an experimental manifestation of the absolute instability.

This paper studies the capillary-driven absolute instability of compound jets. In its base state, a compound jet comprises an inner core fluid of radius R_1 surrounded by an annulus of another fluid, immiscible with the first, of radius R_2. The jet is moving in the axial direction with velocity v. The two interfaces provide destabilizing capillary forces which can cause unstable fluid motions and drop formation: the inner interface between the two immiscible liquids has interfacial tension σ_1 and the outer liquid/gas surface has surface tension σ_2. Compound jets find application in the same fields as single jets, but they have the added flexibility of having two fluids and two interfaces whose physical properties can be manipulated in order to get the desired drop breakup size and breakup distance from the nozzle. The initial motivation for stability studies of compound jets was Hertz and Hermanrud's (Hermanrud 1981; Hermanrud & Herz 1979; Hertz & Hermanrud 1983) investigation for improving ink jet printing. Their experiments showed that compound jets are unstable to capillarity at low and moderate velocities, which is our focus; at very high velocities, other non-axisymmetric varicose and sinuous instabilities predominate. Current interest in compound jets arises from their use in producing compound fibres and spherical compound particles or encapsulation (Kendall 1966; Lee & Wang 1989), gas adsorption or atomization

(Baird & Davidson 1962; Shen & Li 1996) and particle/cell sorting (Hertzberg *et al.* 1976).

The temporal stability of a compound static thread was first studied in the limit in which the core and annular fluids are inviscid, and the axial velocity and pressure in both the fluids are independent of the radial and the azimuthal directions (Radev & Shkadov 1985; Sanz & Masseguer 1985). These one-dimensional temporal analyses for axisymmetric disturbances found two growing modes. One mode is driven by the destabilizing capillary forces at the outer surface $r = R_2$, and becomes unstable for wavelengths larger than the outer circumference. The second is driven by the destabilizing forces at the inner interface $r = R_1$ and is unstable to the waves longer than this circumference. Sanz & Masseguer (1985) demonstrated that the mode driven by the inner interface has an amplitude ratio which is positive, indicating a stretching vibration, while the mode driven by the outer interface has a negative amplitude ratio, and hence is a squeezing vibration. Both groups found that the growth rates of the stretching are much larger than those of the squeezing mode, for all wavenumbers and parameters investigated; thus the stretching mode dominates the linear dynamics. Radev & Tchavdarov (1988), Shkadov & Sisoev (1996) and Chauhan *et al.* (2000) included viscous effects and full axisymmetric motion (i.e. radial as well as axial motions) in a temporal linear stability analysis for a base state of a circular compound jet moving with a uniform velocity v. They found that all of these characteristics carry over. As in the single jet, the disturbances convect with the base velocity, $s_i = -ikv$. Chauhan *et al.* (2000) numerically considered the effects of the system parameters on the maximum growth rate and its corresponding wavelength and amplitude ratio. The parameters considered are the viscosity, density and surface tension ratios of the outer-to-inner fluids. They analytically examined compound jet stability in the limits of long waves and/or thin films. For asymptotically thin annular films the squeezing mode disappears as the square of the ratio ε of film thickness to R_1; the stretching mode becomes independent of film properties and in the limit depends only on the sum of the two interfacial tensions.

Chauhan *et al.* (1996) provided the first insight into the spatial analysis of the compound jet in the absence of viscosity and gravity. They showed that there are again two spatially growing modes and, as in the single jet, these merge with the temporal results set in a travelling frame at high Weber numbers. One (the primary) mode is unstable for $\omega R_1/v$ from 0 to approximately 1 and the other (the secondary) from 0 to approximately R_1/R_2, with the exact values depending on V. However, for finite velocities, these modes are no longer purely stretching or squeezing. The wavelength and growth rate of the convective instability are functions of the surface tension, thickness and density ratios.

The questions that remain are: (i) At what critical values V_{crit} of the Weber number does a compound jet become absolutely unstable? (ii) How does this critical Weber number V_{crit} depend on these system parameters? We focus primarily on the effect of the surface tension ratio γ. (iii) How do the dominant absolute growth rate and its wavelength vary with the Weber number for $V < V_{crit}$? These unresolved issues are important from the standpoint of applications. A separate issue is that even in single-fluid jets, it is still a matter of debate whether the theoretically predicted absolute instability actually manifests itself experimentally (Lin & Lian 1989; O'Donnell, Chen & Lin 2001). This leads to: (iv) Does the compound jet more easily lend itself to an unequivocal experimental observation of the absolute instability than does the simple jet? A necessary condition for being able to distinguish the absolute from the convective instability is to be able to discern instability characteristics, e.g. growth rate,

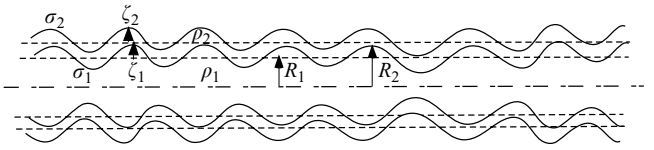

FIGURE 1. Definition sketch of the geometry of the doubly infinite compound jet consisting of a core liquid of density ρ_1 surrounded by an annular fluid of density ρ_2. The interfacial deflection of the core/annular interface with interfacial tension σ_1 is ζ_1 and that of the annular/gas interface with surface tension σ_2 is ζ_2. The undisturbed radius of the core in its cylindrical base state is R_1 and the outer radius of the annular fluid in the cylindrical base state is R_2.

wavelength, dispersion, that may differ between the two. Clearly such measurements require the convective instability to break the jet sufficiently far, i.e. at least a few jet radii ($-k_i a \ll 1$), from the nozzle. For a single-fluid jet of water in air, the critical velocity is low and, since k_i typically scales with $s_r(k_r)/v$, $k_i a$ turns out to be order 1. Does the additional flexibility afforded by the second fluid and fluid/fluid interface change this picture?

Section 2 formulates the linear stability problem and describes the mechanics of finding V_{crit}, the growth rates and wavelengths for the absolute instability from the roots of the dispersion equation. Section 3 calculates these quantities and studies the effect of γ on them. The subsequent section uses these results to identify conditions best suited for the observation of the absolute instability.

2. Formulation of the linear stability theory: governing equations and boundary conditions

A doubly infinite jet of an incompressible, inviscid fluid of density ρ_1 is surrounded by a coaxial annulus of an immiscible, incompressible, inviscid fluid of density ρ_2 (figure 1). Choose a cylindrical coordinate system (r, θ, z), whose z-axis is coincident with the fluid cylinder's axis. The compound jet is moving in a vacuum with a uniform velocity in the positive z-direction. The undeflected inner interface is $r = R_1$ and the outer interface is $r = R_2$. The interfacial tensions are σ_1 and σ_2, respectively.

The equations of motion and continuity in dimensionless form are

$$\nabla \cdot \boldsymbol{v}_i = 0, \qquad i = 1, 2, \tag{1}$$

$$\beta_i \frac{\mathrm{D}\boldsymbol{v}_i}{\mathrm{D}t} = -\nabla P_i, \qquad i = 1, 2, \tag{2}$$

where in fluid i, P_i is the pressure and $\boldsymbol{v}_i$ is the velocity vector. In the governing equations and the boundary conditions, we non-dimensionalize lengths by $[R_1]$, time by $[(\sigma_1/\rho_1 R_1^3)^{-1/2}]$, pressure by the surface tension pressure $[\sigma_1/R_1]$ and velocity by $[(\sigma_1/\rho_1 R_1)^{1/2}]$. The non-dimensional parameters are $a = R_2/R_1$, $\gamma = \sigma_2/\sigma_1$, $\beta_2 = \beta = \rho_2/\rho_1$ and $\beta_1 = 1$. The interfaces are denoted by $r = h_i(z, t)$ $(i = 1, 2)$ and their derivatives with respect to z by $h_i'(z, t)$. Define the mean curvature H_i of interface i $(i = 1, 2)$ by

$$2H_i = -\frac{1}{h_i\left(1 + h_i'^2\right)^{1/2}} + \frac{h_i''}{\left(1 + h_i'^2\right)^{3/2}}. \tag{3}$$

The centreline condition is $\boldsymbol{v}_1$, P finite at $r = 0$; the non-dimensional boundary (the jump in the normal stress and the continuity of normal velocity) and kinematic

conditions at the interfaces are

$$[[P]]_i = -2H\gamma_i + \lambda\delta(z - z_0)\delta(t) \text{ at } r = h_i(z,t), \quad i = 1,2, \tag{4}$$

$$\left[\frac{\partial}{\partial t} + \boldsymbol{v}_i \cdot \nabla\right](r - h_i) = 0 \text{ at } r = h_i(z,t) \quad i = 1,2, \tag{5}$$

$$[[\boldsymbol{n} \cdot \boldsymbol{v}]]_i = 0 \text{ at } r = h_i(z,t), \tag{6}$$

where $[[\ ]]_i$ denotes the difference between the inside and outside of interface i, $\boldsymbol{n}$ is the outward unit vector normal to the interface and the system is responding to an impulse disturbance $\delta(t)$ at $z = z_0$ of size $\lambda \ll 1$. If one were interested in the convective instability, in practice one would replace $\delta(t)$ in (4) with an order one temporal forcing $f_i(t)$ in the pressure applied on surface i at $z = z_0$, by, say, nozzle tip imperfections. We take $z_0 = 0$, i.e. the source's position defines the origin. The initial conditions are zero interfacial deflections and a uniform flow. The reason for this choice of forcing and initial condition is that we are interested in instabilities that arise from instantaneous disturbances at the nozzle tip, because this corresponds best to the experimental situation of a jet issuing from a nozzle. In contrast, a free-standing jet responds to an initial disturbance with spatial structure, which is more applicable to static jets and threads.

In the base state there is no forcing, and the interfaces are undeflected. Let u and w denote the radial and axial velocities, respectively. Any velocity solution of the form $u = 0$, $w = \Phi(r)$, $\Phi(r)$ twice differentiable but otherwise completely arbitrary, satisfies the base state equations (1)–(6) exactly. Since we are interested in capillary-driven instabilities, we restrict the analysis to solutions in which $w = \text{constant} = V$ in both the core and the annulus. With this assignment, there is no slip at the interface in the base state, thereby preventing the Kelvin–Helmoltz (Chandrasekhar 1961) type of instability. Thus, we concentrate on the base state (superscript (o)):

$$u_i^{(0)} = 0,\ w_i^{(0)} = V, \quad i = 1,2, \tag{7}$$

$$P_2^{(0)} = \frac{\gamma}{a}, \quad P_1^{(0)} = 1 + \frac{\gamma}{a}. \tag{8}$$

The induced disturbances to the velocities and the interface from the base state are also of order λ. For $i = 1, 2$,

$$u_i(r,z,t) = u_i^{(1)}(r,z,t)\lambda + O(\lambda^2), \tag{9a}$$

$$w_i(r,z,t) = V + w_i^{(1)}(r,z,t)\lambda + O(\lambda^2), \tag{9b}$$

$$h_1(z,t) = 1 + \zeta_1^{(1)}(z,t)\lambda + O(\lambda^2), \tag{10}$$

$$h_2(z,t) = a + \zeta_2^{(1)}(z,t)\lambda + O(\lambda^2), \tag{11}$$

$$P_i(r,z,t) = P_i^{(0)} + P_i^{(1)}(r,z,t)\lambda + O(\lambda^2). \tag{12}$$

Substituting these in the governing equations, one gets the leading-order equation for the perturbation quantities,

$$\beta_i\left(\frac{\partial \boldsymbol{v}_i}{\partial t} + V\frac{\partial \boldsymbol{v}_i}{\partial \boldsymbol{z}}\right) = -\nabla P_i, \quad i = 1,2, \tag{13}$$

$$\nabla \cdot \boldsymbol{v}_{\mathrm{i}} = 0, \quad i = 1,2, \tag{14}$$

where we delete superscript (1) denoting the perturbation order. Taking the divergence of the momentum balance and using the equation of continuity, we get

$$\nabla^2 P_i = 0. \tag{15}$$

Define the Fourier–Laplace transforms as

$$\hat{g}(s,k) = \int_{-\infty}^{\infty} \mathrm{e}^{-\mathrm{i}kz} \left\{ \int_{0}^{\infty} \mathrm{e}^{-st} g(t,z)\,\mathrm{d}t \right\} \mathrm{d}z. \tag{16}$$

In the transformed domain, equation (15) becomes

$$\left[\frac{\mathrm{d}^2}{\mathrm{d}r^2} + \frac{1}{r}\frac{\mathrm{d}}{\mathrm{d}r} - k^2 \right] P_i(r,k,s) = 0, \tag{17}$$

where we delete the 'hat' so that $P_i(r,k,s)$ is the pressure in the Fourier–Laplace domain. The general solution of (17) is

$$P_i = A_i I_0(kr) + B_i K_0(kr) \tag{18}$$

where I_0 and K_0 are the modified Bessel functions of order 0 and A_i, B_i are constants of integration which can be functions of k and s but not of r.

The boundary and kinematic conditions (4)–(6) in dimensionless form in the Fourier–Laplace domain are

$$P_2 = -\gamma \left(\frac{1}{a^2} - k^2 \right) \zeta_2 + 1 \quad \text{at } r = a, \tag{19}$$

$$P_1 - P_2 = -(1-k^2)\zeta_1 + 1 \quad \text{at } r = 1, \tag{20}$$

$$u_1 = s\zeta_1 \quad \text{at } r = 1, \tag{21}$$

$$u_1 = u_2 \quad \text{at } r = 1, \tag{22}$$

$$u_2 = s\zeta_2 \quad \text{at } r = a. \tag{23}$$

If one focused on the convective instability the term 1 on the right of (19), (20), (24) would be replaced by the Laplace transform $F_i(s)$ of $f_i(t)$, $i = 1, 2$. The velocity and pressure are finite at $r = 0$.

Using (13) to get $u_i(r,k,s)$ and substituting for u_i and P in (19)–(23) yields $\boldsymbol{A}(k,s)\boldsymbol{x} = \boldsymbol{b}(k,s)$,

$$\boldsymbol{b}^t = [0, 0, 0, 1, 1], \tag{24}$$

$$\boldsymbol{x}^t = [A_1, A_2, B_2, \zeta_1, \zeta_2], \tag{25}$$

$$\boldsymbol{A}(k,s) = \begin{pmatrix} I_1(k) & -\dfrac{I_1(k)}{\beta} & \dfrac{K_1(k)}{\beta} & 0 & 0 \\ kI_1(k) & 0 & 0 & (s+\mathrm{i}kV)^2 & 0 \\ 0 & \dfrac{kI_1(ka)}{\beta} & \dfrac{-kK_1(ka)}{\beta} & 0 & (s+\mathrm{i}kV)^2 \\ 0 & I_0(ka) & K_0(ka) & 0 & \gamma\left(\dfrac{1}{a^2} - k^2\right) \\ I_0(k) & -I_0(k) & -K_0(k) & (1-k^2) & 0 \end{pmatrix}. \tag{26}$$

The solution of this system of five equations for ζ_1 and ζ_2 is

$$\zeta_1 = \frac{1}{|\boldsymbol{A}|}[C_{44} + C_{45}], \tag{27}$$

$$\zeta_2 = \frac{1}{|\boldsymbol{A}|}[C_{54} + C_{55}], \tag{28}$$

where $|\boldsymbol{A}|$ is the determinant of the matrix $\boldsymbol{A}$ (26) whose (mn)th element is a_{nm}, with corresponding cofactor C_{mn}. Again, for convective, instabilities the brackets in (27)–(28) would be $[C_{j4}F_2 + C_{j5}F_1]$, $j = 4, 5$, respectively, and one would choose a periodic forcing, say, at the outer interface only, such as $f_1(t) = 0$ and $f_2(t) = F\sin(\omega_0 t)$ or $F\cos(\omega_0 t)$, $F_2(s) = F\omega_0/(s^2 + \omega_0^2)$ or $Fs/(s^2 + \omega_0^2)$, denominators typical for the signalling problem. It is clear from (26) (Chauhan *et al.* 2000, 1996) that $|\boldsymbol{A}|$ is a quadratic form in $(s + \mathrm{i}kV)^2$ and, as such, the dispersion equation $|\boldsymbol{A}| = 0$ has four solutions $s_j(k)$, $j = 1, \ldots 4$.

To get the solution in the time and space domain, one must invert the solution from the Fourier–Laplace domain, i.e.

$$\begin{aligned}\zeta_i(z,t) &= \frac{1}{4\pi^2\mathrm{i}}\int_{c-\mathrm{i}\infty}^{c+\mathrm{i}\infty} \mathrm{e}^{st}\left[\int_{-\infty}^{+\infty}\zeta_i(k,s)\mathrm{e}^{\mathrm{i}kz}\,\mathrm{d}k\right]\mathrm{d}s \\ &= \frac{1}{4\pi^2\mathrm{i}}\int_{-\infty}^{+\infty}\mathrm{e}^{\mathrm{i}kz}\left[\int_{c(k)-\mathrm{i}\infty}^{c(k)+\mathrm{i}\infty}\zeta_i(k,s)\mathrm{e}^{st}\,\mathrm{d}s\right]\mathrm{d}k, \end{aligned} \tag{29}$$

where we can perform the integrals as complex-plane contour integrations in either order. With s as the inner integral, $c(k)$ is a real number that for the given k lies to the right of all singularities of ζ_i in the s-plane; with s as the outer integral, c simply lies (see below) to the right of the maximum temporal growth rate. The integrations involve determining the poles and corresponding residues of the inner integrand as a function of the outer variable of integration. These become the integrand of the outer contour integral (Bers 1983; Briggs 1964; Huerre & Monkewitz 1990; Rudin 1987). Naturally the branch cuts of the integrands must be carefully considered during this process.

If we choose the k-integral as the inner one, the absolute instability arises from singularities of the poles of the k-residues as functions of s in the portion of the s-plane composed of the s-plane contour and its interior, i.e. to the left of the vertical line $(c - \mathrm{i}\infty,\ c + \mathrm{i}\infty)$, i.e. $S_r = c$. The k-plane residues involved derive from those k-plane singularities that lie in the upper-half k-plane when $s_r = c$ and exclude all others. (A sinusoidal forcing, absent in our problem, would generate two s-plane singularities on the imaginary s-axis at $\pm\mathrm{i}\omega_0$ that can only contribute growth in z (convective instability) since $s_r = 0$. It does so when the continuation of a k-plane residue that lies in the upper-half k-plane for s on $S_r = c$ migrates to the lower-half k-plane for $s = \pm\mathrm{i}\omega_0$, i.e. when evaluated as part of the residue at this pole.) Singularities deriving from k-plane residues originating from the dispersion relation can contribute exponential growth in time, i.e. absolute instability, if they occur for $s_r > 0$, and we call any such singularity for $s_r > 0$, not just the one with largest s_r, an absolute instability. These arise by the merger (to form higher-order poles) at s_r such that $c > s_r > 0$ of k-plane poles, at least one of which is and at least one of which is not included in the s-integrand, i.e. that for $s_r = c$ have k_i of opposite signs. A merger of roots occurs in the k-plane at k^* when $\partial|A(k,s)|/\partial k = 0$. This merger is the point where the analytic continuation, accomplished by the continuous deformation of the inner k-integral's contour that encloses one but not the other of these roots, becomes singular (Bers 1983; Briggs 1964; Huerre & Monkewitz 1990). Thus the calculations for the figures focus on following the locations/motions of these poles in the k-plane as s_r changes, and carefully tracks the merge points back to large $s_r > 0$.

To determine c, note that at the points at which a root crosses the real k-axis, the dispersion equation takes the form $s_n + \mathrm{i}kV = g_n(k)$. Here $g_n(k)$ is the temporal growth rate of the nth mode, where Chauhan *et al.* (1996) show that this dispersion equation

is a quadratic in $(s + \mathrm{i}kV)^2$, thus having precisely four roots, i.e. $n = 1, 2, 3, 4$. They use the form of the dispersion equation that is explicit in s to show that the temporal growth is either purely real or purely imaginary for k real. Thus, if s_r is greater than the maximum temporal growth rate ($\max(g_n(k))$) for the corresponding mode, there can be no solution to $s_n = g_n(k) - \mathrm{i}kV$ and $k(s)$ cannot intersect the real k-axis. For each mode, this is then the minimum value for c.

As suggested by Briggs, we catalogue the mergings by beginning with a value of s_r equal to the minimum value of c and plotting the branches of $k(s_r - \mathrm{i}\omega) : \omega > 0$, and then lowering s_r, eventually to zero. During this process, branches of $k(s)$ that begin above and below the real k-axis may merge, and the order of which branches merge with which constitutes the merging pattern. By examining the matrix in equation (26), one can show that the dispersion equation $\phi(s, k; V) = |\boldsymbol{A}|$ satisfies the symmetries $\phi(s, k; V) = \phi(s^*, k^*; -V)^*$ and $\phi(s, k; V) = -[\phi(s^*, -k^*; V)]^* = [\phi(-s^*, k^*; V)]^*$, where $*$ denotes complex conjugate. Thus if $\phi(s_r + \mathrm{i}\omega, k_r + \mathrm{i}k_i; V) = 0$, then $\phi(s_r - \mathrm{i}\omega, -k_r + \mathrm{i}k_i; V) = 0$, or for a given s_r the solution for $s_i = -\omega$ is a mirror image of $s_i = \omega$ about the imaginary k-axis. This symmetry permits us to only inspect $\omega > 0$, i.e. $s_i < 0$. Also, if $s_r = 0$, $s^* = -s$. Hence if $\phi(\mathrm{i}\omega, k_r + \mathrm{i}k_i; V) = 0$, then $\phi(\mathrm{i}\omega, k_r - \mathrm{i}k_i; V) = 0$ or, for purely imaginary s, the solutions in the upper and lower-half k-planes are mirror images.†

3. Results and discussion

3.1. *Calculation of the critical velocity (Weber number) V_c and the growth rates below V_c*

Our first goal is to locate the critical velocity at a fixed γ. Then we investigate how the growth rate of the absolute instability varies by further lowering the Weber number at constant γ. We do this in a rational way by following all the mergings (see the Supplementary Material) that occur for $s_r > 0$, rather than restricting ourselves to the one occurring at the largest value of s_r. The full catalogue of mergings may also be a first step in a nonlinear analysis should some or all of the linearly absolutely unstable modes saturate in the nonlinear regime.

From this catalogue of merging patterns one can construct a phase diagram (figures 2–5), i.e. a plot of the simultaneous solutions of $|A(k, s)| = 0$ and $\partial|A(k, s)|/\partial k = 0$ having $s_r \geqslant 0$, which synthesizes the absolutely unstable k and s values as a function of the non-dimensional velocity V. In particular, they provide a picture of the change (upon reduction of s_r) in the sequence of the merging patterns. The demarcations shown by vertical dashed lines in the figures are the values of V at which the order of the merging patterns change and they identify the first four regions. The discussion in the Supplementary Material describes the patterns for each of these regions. Region V is distinguished from region IV not for this reason, but rather because in region V, the second merging is no longer absolutely unstable. As figure 3 shows, this demarcation is the value of V at which the s_i values for the first and second mergings are equal. (The Supplementary Material follows the four roots of the dispersion equation as functions of s_i at fixed s_r which, for large s_r, are labelled roots [1]–[4]. Roots [1] and [2] descend and [3] and [4] rise as one decreases s_r. These roots can merge and split, e.g. [1] and [4] can merge and split into [14], whose small (large) $-s_i$ portion is a continuation of root [1] ([4]) and [41], as s_r decreases. In

† These patterns are followed in detail for different Weber numbers in a supplement to the online version of this paper, which is also available from the authors or the JFM Editorial Office.

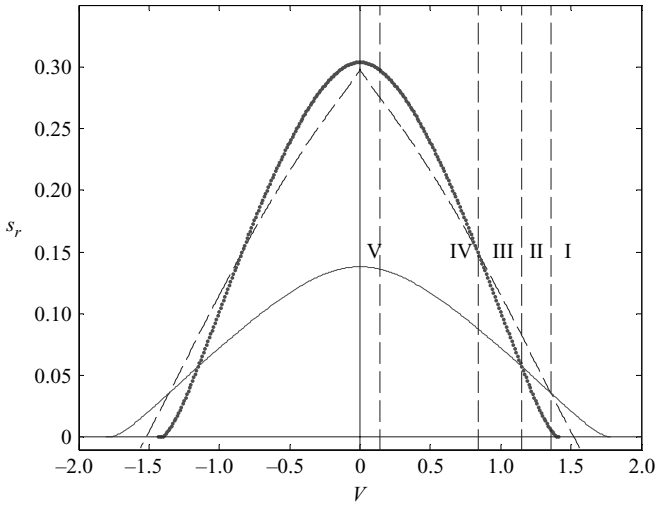

FIGURE 2. For each V between -2 and 2 there are between zero and three mergings, i.e. simultaneous solutions of $|\boldsymbol{A}(k, s)| = 0$ and $\partial|A|/\partial k = 0$ having $s_r > 0$, of roots of the dispersion equation when each is plotted, as in the Supplementary Material, in the k-plane as a curve parameterized by s_i at fixed s_r as s_r decreases from any value greater than the maximum temporal growth rate to 0. The three curves show s_r as a function of V at these points of merging. Roman numeral demarcations indicate regimes in V, each with a distinct merging pattern, that give rise to the absolute instability. $a = 2$, $\beta = 1$ and $\gamma = 2$.

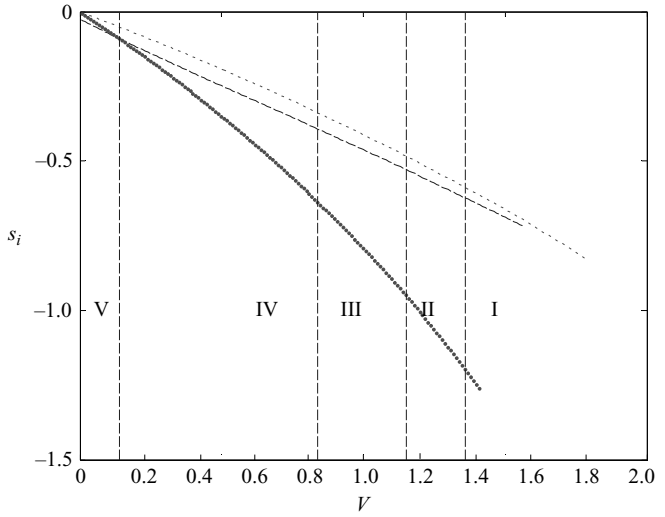

FIGURE 3. As figure 2 but showing curves of s_i as a function of V.

terms of these details, the s_i value at which the first and second mergings are equal means the value at which the second merging changes from being between root [3] and the root-[1] part of [14] to being between root [3] and the root-[4] part of [14]. Consequently, the subsequent merging with [2] shifts from [143] to [314].)

Certain regularities in figures 2–5 are apparent. As a result of the symmetries of (26) above, the curves in figures 2 and 4 are symmetric and those in figures 3 and 5

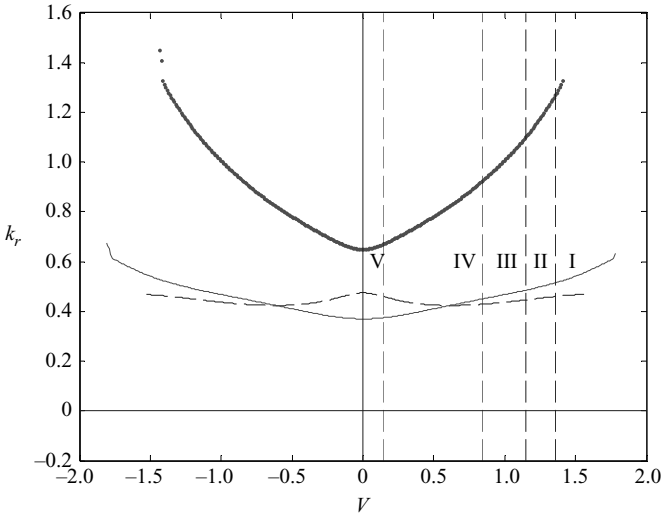

FIGURE 4. Curves of k_r as a function of V for the points of absolute instability shown in figures 2 and 3. Bold dotted, dashed and light-dotted curves correspond to similarly labelled curves in figures 2 and 3. $a = 2$, $\beta = 1$ and $\gamma = 2$.

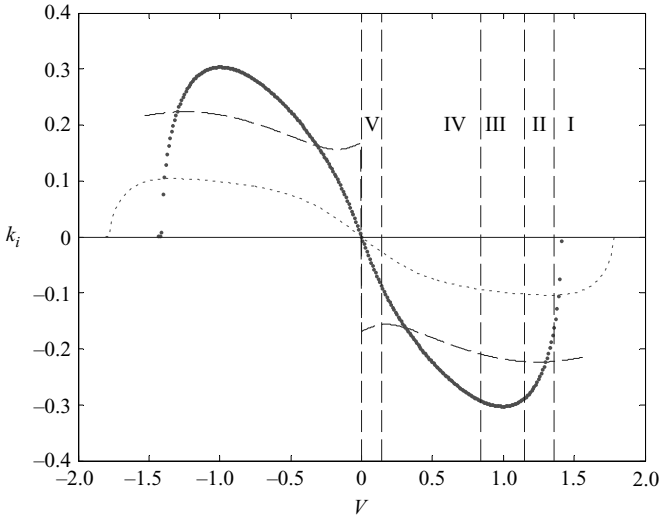

FIGURE 5. Curves of k_i as a function of V for the points of absolute instability shown in figures 2 and 3. Bold dotted, dashed and light-dotted curves correspond to similarly labelled curves in figures 2 and 3. $a = 2$, $\beta = 1$ and $\gamma = 2$.

are anti-symmetric ($V < 0$ not shown in figure 3) about $V = 0$. In particular, figure 2 indicates that two of the curves (the dotted ones) have zero slope at $V = 0$ whereas the third (dashed) has a (symmetric) cusp there. All three of these curves intersect the $s_r = 0$ axis for finite V values, but only the curve having the cusp at $V = 0$ intersects the $s_r = 0$ axis transversely, while the others intersect it tangentially and remain on the V-axis for all higher values of V. That they remain on the V-axis reflects the fact that for V greater than these intersection values (where the curves no longer

represent absolute instability, a condition that would require $s_r > 0$ at merging), there is nevertheless always a merging of roots of the dispersion equation on the real k-axis for $s_r = 0$.

Figure 4 shows that the k_r values corresponding to the $s_r = 0$ V values are greater than (approximately) 1 and $1/a$, the critical wavenumbers k_r values for each mode that divide convectively growing ($k_i < 0$ for $V > 0$) from decaying waves. This is consistent with what we know from the temporal analysis: that on the real k-axis, k_r greater than a cutoff (close to 1 or $1/a$, depending on the mode) yields s purely imaginary. The remaining mode retains $k_i < 0$ for V such that $s_r < 0$, but the exponential decay in time overwhelms its spatial growth. From figure 5, a plot of the absolutely unstable and axial growth rate k_i corresponding to the curves from figures 2 and 3, one can see that the two dotted curves both have $k_{ia} = 0$, i.e. are not also convectively unstable and have no growth in z, both for $V = 0$ and for the V value at which they intersect the $s_r = 0$-axis.

Let us examine the relationship between $\mathrm{d}s/\mathrm{d}V = 0$ and $k_i = 0$ more closely. Recall that the conditions (for the merging of roots) that generated the curves in figures 2–5 were $|\boldsymbol{A}(s, k; V)| = 0$ and $\partial|\boldsymbol{A}(s, k; V)|/\partial k = 0$. Since $\mathrm{d}|\boldsymbol{A}(s(k), k; V)|/\mathrm{d}k = \partial|A(s, k; V)|/\partial k + (\partial|A(s, k; V)|/\partial s)\ (\partial s(k, V)/\partial k) = 0$, if $\partial|A(s, k; V)|/\partial s \neq 0$ then $\partial s(k, V)/\partial k = 0$. Recall also that the solution of the dispersion equation $|\boldsymbol{A}(s, k)| = 0$, a quadratic in $(s + \mathrm{i}kV)^2$, can also be written in the form $s + \mathrm{i}kV = g(k)$. Thus, if the absolutely unstable s is considered a function of k, which depends on V, i.e. $s = s(k(V), V)$, then for the curves in figures 2–5, $\mathrm{d}s/\mathrm{d}V = (\partial s/\partial k)(\mathrm{d}k/\mathrm{d}V) + \partial s/\partial V = -\mathrm{i}k$, or $\partial s_r/\partial V = -\mathrm{i}k_i$ and $\partial s_i/\partial V = -k_r$. Thus $\mathrm{d}s_r/\mathrm{d}V = 0$ exactly when $k_i = 0$, as is the case for the two dotted curves at $V = 0$ and where they intersect the V-axis. In contrast, the dashed curve has non-zero slopes and non-zero k_i both at $V = 0$ and at its crossing of the V-axis. Moreover, at $V = 0$, $\partial s(k, V)/\partial k = g'(k) = 0$, where k and s are both real, for the two dotted curves. This equation defines the maximum growth rate of the temporal stability problem, whose two unstable modes consist of motions of the two interfaces that are either in-phase, the so-called stretching mode, and out-of-phase, the so-called squeezing mode. Numerical and asymptotic investigation of the temporal problem strongly suggests that the stretching mode always has the larger growth rate, and thus we identify the denser dots with the former and the sparser dots with the squeezing modes.

Note that if $\partial s(k, V)/\partial k = 0$, i.e. $g'(k) = \mathrm{i}V$, then the solution of this implicit equation for k would be clearly V-dependent. Thus, $k \neq k(V)$, i.e. $k_i(V)$ and $k_r(V)$ both flat for $V > 0$, would imply $\partial s(k, V)/\partial k \neq 0$, and so $\partial|\boldsymbol{A}(s, k; V)|/\partial s = 0$. Together with $|\boldsymbol{A}(s, k; V)| = 0$, this provides an implicit equation for the V-independent k value. $s + \mathrm{i}kV = g(k)$ would then imply that the dashed curves in figures 2 and 3 would be straight lines. Note that these curves are almost straight and the dashed curves in figures 4 and 5 are almost flat. As shown in the Supplementary Material, this indicates that the mergers corresponding to the dashed curves indeed take place near, but not at, the points where $\partial|A(s, k; V)|/\partial s = 0$, which turn out to be branch points. This suggests that with a little tuning of the system parameters, e.g. γ and/or a, one could arrange for the merging to take place at the branch point.

The outer envelope in figure 2 defines the dominant growth rate of the absolute instability. Clearly its slope is discontinuous due to different mergings dominating in different regions. Consequently, at the boundaries of these regions, the dominant wavelength k_r and axial growth k_i can change discontinuously as one switches from one branch of figure 2 to another at a region boundary crossing. See figures 4 and 5. It is important to stress here that the merging patterns displayed in figures 2 and

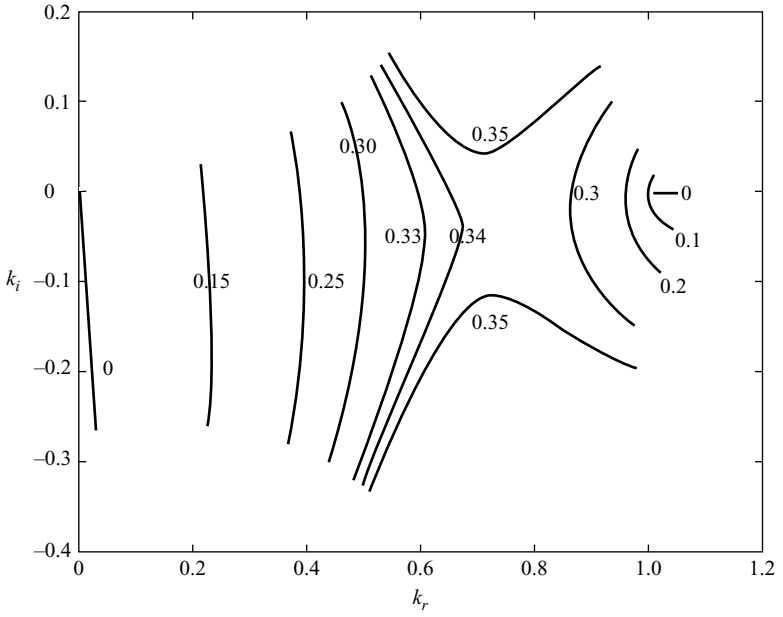

FIGURE 6. Curves in the k-plane of constant s_r and varying s_i ($=-\omega$) for roots lying in the upper and lower k-plane for large s_r for a single jet for V smaller than the critical value of 1.77. There exists only one merging pattern.

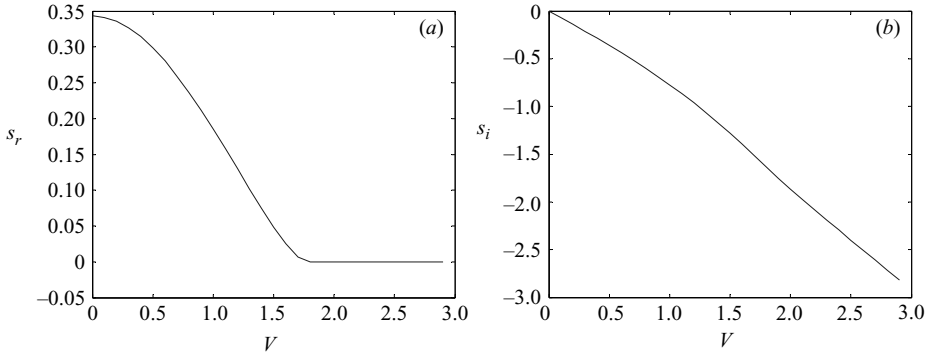

FIGURE 7. Curves of s_r (a) and s_i (b) as a function of V at the point of absolute instability (simultaneous solutions of $|\boldsymbol{A}(k,s)|=0$ and $\mathrm{d}s/\mathrm{d}k=0$ having $s_r \geqslant 0$) for a single jet. Only one locus exists because of the single merging pattern.

3, as well as its outer envelope, are strong functions of the system parameters, e.g. a and γ, and must therefore be calculated for each specific parameter set.

These discontinuities of k_r and k_i in the dominant mode below the critical Weber number occur in the compound jet but not in the single jet. Let us compare these results to the single jet's. The single-jet dispersion equation is simply $(s+\mathrm{i}kV)^2 = k^2(1-k^2)I_1(k)/I_0(k)$ and figure 6 shows the only merging pattern below the critical $V=1.77$ (Leib & Goldstein 1986*b*; Lin & Lian 1989). Correspondingly, there is only one dominant mode (and no discontinuity in k_r or in k_i), which figure 7 displays in analogy to figures 2 and 3, i.e. s_r and s_i vs V. Again, above the critical value of V the merging occurs for $s_r=0$, i.e. the curve in figure 7(a) continues along the V-axis,

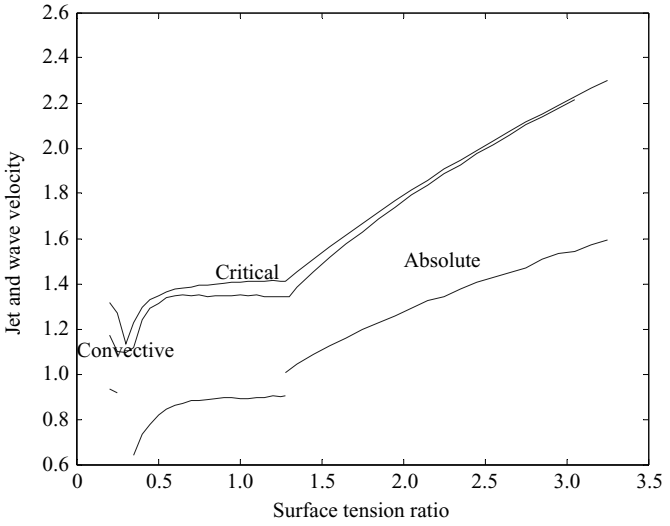

FIGURE 8. Effect of the surface tension ratio γ on the critical Weber number V (labelled 'critical'); the absolute wave velocity given by $-s_{ia}/k_{ra}$ evaluated at the critical velocity; and the convective wave velocity ω_{max}/k_{rmax} at the maximum spatial growth rate $-k_{imax}$. $a = 2$ and $\beta = 1$.

and lies on the real k-axis to the right of the k_r that demarcates the beginning of the convectively growing waves. For $V = 0$, the merging again takes place on the real k-axis as in the compound jet.

3.2. *Effect of the surface tension ratio on the critical V*

As already remarked, the merging patterns above change significantly with a change in system parameters β, γ and a. Because the instability is driven by surface tension, the most important of these is the surface tension ratio, γ. Figure 8 shows the effect of the surface tension ratio on three parameters: (i) the critical Weber number of the compound jet; (ii) the wave velocity s_{ia}/k_{ra} of the absolute instability at V_{crit}; and (iii) the wave velocity s_i/k_r of the convectively growing wave with the largest $-k_i$. As with changing V, different modes become dominant in different regimes of γ and this leads to the discontinuities in slope of the critical velocity at $\gamma = 0.3$ and 1.3. Moreover, the values of the critical Weber number are significantly above and below the critical $V = 1.77$ for the single jet.

3.3. *Conditions necessary for the experimental manifestation of the absolute instability*

Despite a growing literature on the theoretical possibility of the absolute instability in jets of a single fluid, this type of instability has defied unambiguous experimental observation. Below we investigate the reason for this difficulty and argue that these difficulties are far less constraining for the compound jet. Thus the compound jet should be much more conducive to such observations.

When absolute instability sets in below the critical velocity, the theory predicts that waves with wavelength $1/k_{ra}$ characteristic of the absolute instability will grow in time everywhere along the jet with growth rate s_{ra}. In contrast, the convective instability, which is present both above and below this critical velocity, grows spatially with a spatial growth rate $-1/k_i$. This k_i is a function of the applied frequencey ω_0 and has a maximum $(-k_i)_{max}$, or simply $-k_{imax}$, at a particular frequency ω_{max} with a corresponding wavelength k_{rmax}. In principle, in order to observe the absolute

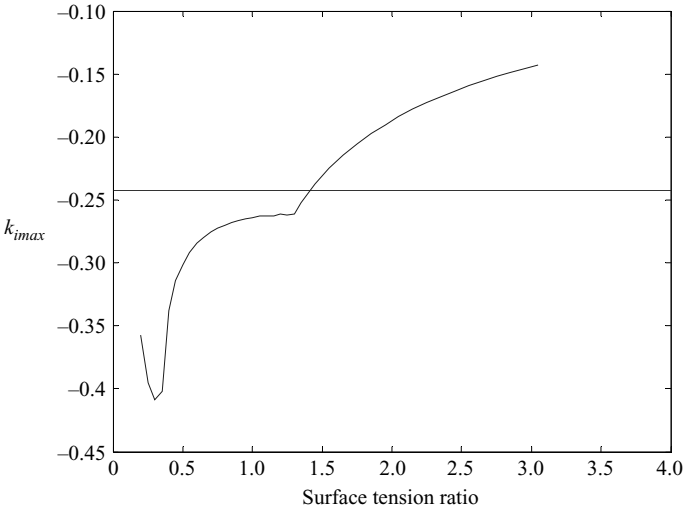

FIGURE 9. Plot of the maximum spatial growth rate k_{imax} as a function of γ at the corresponding critical velocity for absolute instability. $a = 2$ and $\beta = 1$.

instability, it is necessary that the convective instability not break the jet too close to the nozzle ($-1/k_{imax} \gg 1$, k_{imax} non-dimensional) and that the absolute instability be slow enough to allow the jet to first form ($1/s_{ra} \gg 1/V$). This latter criterion is easy to satisfy, since the growth rate s_{ra} of the absolute instability at the critical velocity is zero, and increases continuously below V_{crit} (figure 2). The scenario envisioned is for the jet to form clearly and initially break convectively with wavenumber k_{rmax}. Then, on a slower time scale $1/s_{ra}$ the wavenumber k_{ra} takes over everywhere and the jet breaks with this wave number everywhere (excluding effects close to the nozzle) due to the absolute instability. (Note that the absolute instability also has a convective part $-k_{ia}$ that could, in principle, contribute to the character of the absolute-instability-dominated part of the break up.)

For the single-fluid jet at the critical value $V_{crit} = 1.77$, $-k_{imax} = 0.243$, which, when accounting for the nozzle effects may not allow a long enough jet to discern breakup everywhere in its domain. In contrast, in the compound jet, the value of $-k_{imax}$ is a function of the system parameters, and (figure 9) a choice of fluids with a surface tension ratio larger than one can easily give $-k_{imax}$ below 0.15, thereby facilitating a longer intact jet. Given an existing compound jet, one would then look for characteristics that distinguish the absolute relative to the convective instability. The easiest characteristic to observe is the wave length of the growing wave. Unfortunately, according to figure 10, the wave lengths of the absolutely unstable waves at high γ–where the convective growth rate is the slowest and thereby fosters extended intact jets–do not distinguish themselves significantly from the convectively unstable wavelengths. However, the regime where these two wavelengths will be significantly different, with the absolute waves being significantly shorter (about half) than the convective waves, is at lower surface tension ratios where k_i for the compound jet is similar to that for the single jet. If at these k_i values it is indeed possible to form sufficiently long intact single and double jets, the wavenumber disparity for the compound jet (see figure 10) is a factor of 2, whereas for the single jet (not shown) it is closer to 1.5. Another potentially distinguishing characteristic is the wave speed of the absolute instability relative to that of the dominant convectively growing waves.

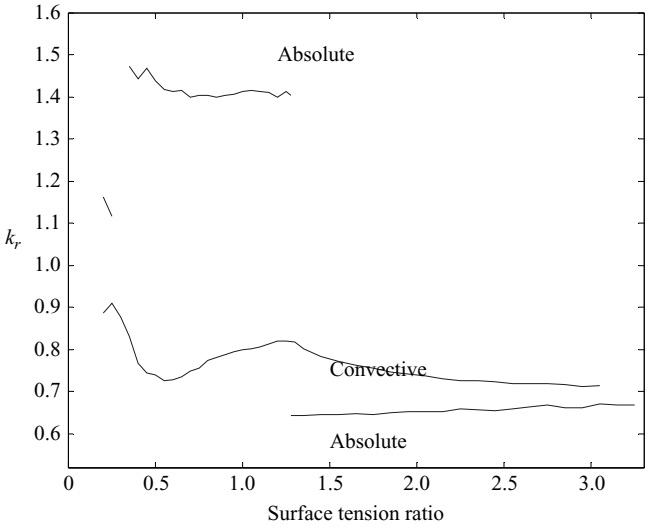

FIGURE 10. Plot of the effect of the surface tension ratio on the convective wavenumber k_{rmax} at the conditions of maximum spatial growth at the critical velocity for absolute instability; and on the wavenumber k_{ra} of the absolute instability at the critical velocity. $a = 2$ and $\beta = 1$.

Figure 8 shows that although the maximally growing convectively unstable waves travel with the jet essentially at the jet's critical velocity, the absolutely unstable waves at the critical velocity travel significantly slower. Thus one might be able to observe short, absolute waves travelling significantly slower than the jet.

One final note: figures 8 and 10 display curves that are only piecewise continuous. Just as in figure 9 where they led to curves with piecewise continuous slopes, changes in γ change the values at which the curves of root mergings cross the $s_r = 0$-axis. At particular values of the surface tension ratio, the particular curve (the 'dominant' one) that crosses for the highest velocity, thereby determining V_{crit}, can change and thus change the observable characteristics there.

4. Conclusions

In addition to being convectively unstable at all Weber numbers, the inviscid compound jet is also absolutely unstable below a critical velocity. This critical velocity is a function of the jet parameters: the ratios of densities, surface tensions and radii of the two interfaces. We focus on the surface tension ratio and find that the critical velocity can be either less than or greater than the value 1.77 for the single jet with the same radius and density of the inner fluid and a surface tension equal to the fluid–fluid tension of the compound jet. At $V = 0$, the absolute instability recovers the maximum growth rate of the standard temporal analysis.

The absolute instability arises from certain roots of the dispersion equation that have multiplicity greater than one. In the compound jet there are at least three such roots and for sufficiently low velocities one or more of these has positive growth rate s_r in time. As one varies the system parameters, say γ, the root that attains positive s_r for the largest velocity (thereby determining V_{crit}) can change. This change leads to discontinuities in the wavelength and wave speed of the absolute instability at criticality. At different values of V at fixed γ, there may be multiple non-simple roots with positive s_r, and the one with the largest positive s_r will dominate the

(linear) growth. This leads to a plot of the growth rate s_r of the absolute instability as a function of the non-dimensional jet velocity V whose slope is only piecewise continuous. These discontinuities are absent in the single fluid jet.

We have determined that a compound jet with surface tension ratio γ greater than one should lead to a jet that is susceptible to breakup by the convective instability at longer non-dimensional distances from the jet nozzle than the single-fluid jet, but the wavelength of the absolutely growing wave at this surface tension ratio is similar to that of the convectively growing wave. At lower surface tension ratios the absolutely growing waves are about half the size of the convectively growing ones, but the length of the jet before convective breakup is comparable to that in the single-fluid jet. It is hoped that these insights may facilitate the observation of the absolute instability for non-dimensional jet velocities just below criticality, a task that has thus far proven elusive for the single-fluid jet.

We thank Air Force Office for Scientific Research (F49620-94-1-0242 to DP), National Science Foundation (DMS 9-9-0070 to DP, CTS 8658147 to DR) and the donors of the Petroleum Research Fund (ACS-PRF #27403-AC9 to DR) for supporting this work. Additional support for D.T.P. was provided by the National Aeronautics and Space Administration under Contract No. NAS1-19480 while the author was in residence at the Institute for Computer Applications in Science and Engineering (ICASE), NASA Langley Research Center, Hampton, VA 23681-0001. D.R. would also like to thank the Alexander von Humboldt Foundation for providing fellowship support at the Ruhr University of Bochum, where a portion of this work was done.

REFERENCES

Baird, M. H. I. & Davidson, J. F. 1962 Annular jets – I: Fluid mechanics. *Chem. Engng Sci.* **17**, 467–472.

Bers, A. 1983 Space time evolution of plasma instabilities. *Handbook of Plasma Physics*, pp. 451–517. North Holland.

Briggs, R. J. 1964 *Electron Stream Interaction with Plasmas*. MIT Press.

Chandrasekhar, S. 1961 *Hydrodynamic and Hydromagnetic Stability*. Dover.

Chaudhary, K. C. & Maxworthy, T. 1980 The nonlinear capillary instability of a liquid jet. Part 3. Experiments on satellite drop formation and control. *J. Fluid Mech.* **96**, 287–297.

Chauhan, A., Maldarelli, C., Papageorgiou, D. T. & Rumschitzki, D. 2000 Temporal instability of compound threads and jets. *J. Fluid Mech.* **420**, 1–25.

Chauhan, A., Maldarelli, C., Rumschitzki, D. & Papageorgiou, D. T. 1996 Temporal and spatial instability of an inviscid compound jet. *Rheol. Acta.* **35**, 133–149.

Donnelly, R. J. & Glaberson, W. 1966 Experiment on capillary instability of a liquid jet. *Proc. R. Soc. Lond.* A **290**, 547–556.

Goedde, E. F. & Yuen, M. C. 1970 Experiments on liquid jet instability. *J. Fluid Mech.* **40**, 495–511.

Hermanrud, B. 1981 A compound jet. A new method to generate fluid jets for ink printing. PhD thesis, Department of Electrical Engineering. Lund Institute of Technology, Sweden.

Hermanrud, B. & Herz, C. H. 1979 Ink jet development at the Lund Institute of Technology. *J. Appl. Photogr. Engng* **5**, 220–225.

Hertz, C. H. & Hermanrud, B. 1983 A liquid compound jet. *J. Fluid Mech* **131**, 271–287.

Hertzberg, L. A., Sweet, R. G. & Herzberg, L. A. 1976 Fluorescence-activated cell sorting. *Sci. Am.* **234**, 97.

Huerre, P. & Monkewitz, P. A. 1990 Local and global instabilities in spatially developing flows. *Annu. Rev. Fluid Mech.* **22**, 473–537.

Keller, J. B., Rubinow, S. L. & Tu, Y. O. 1973 Spatial Instability of a jet. *Phys. Fluids* **16**, 2052–2055.

KENDALL, J. M. 1966 Experiments on annular liquid jet instability and on the formation of liquid shells. *Phys. Fluids* **9**, 2086–2094.

LEE, C. P. & WANG, T. G. 1989 The theoretical model for the annular jet instability – revisited. *Phys. Fluids* A **1**, 964–967.

LEIB, S. J. & GOLDSTEIN, M. E. 1986*a* Convective and absolute instability of a viscous jet. *Phys. Fluids* **29**, 952–954.

LEIB, S. J. & GOLDSTEIN, M. E. 1986*b* The generation of capillary instabilities on a liquid jet. *J. Fluid Mech.* **168**, 479–500.

LIN, S. P. & LIAN, Z. W. 1989 Absolute instability of a liquid jet in a gas. *Phys. Fluids* A **1**, 490–493.

O'DONNELL, B., CHEN, J. N. & LIN, S. P. 2001 Transition from convective to absolute instability in a liquid jet. *Phys. Fluids* **13**, 2732–2734.

PIMBLEY, W. T. 1976 Drop formation from a liquid jet: a linear one-dimensional analysis considered as a boundary value problem. *IBM J. Res. Dev.* **20**, 148–156.

RADEV, S. & SHKADOV, V. 1985 On a stability of two-layer capillary jet. *Theor. Appl. Mech.* **16**, 68–75.

RADEV, S. & TCHAVDAROV, B. 1988 Linear capillary instability of compound jets. *Intl J. Multiphase Flow* **14**, 67–69.

RAYLEIGH, LORD 1879 On the instability of jets. *Proc. Lond. Math. Soc.* **10**, 4–13.

RUDIN, W. 1987 *Real and Complex Analysis*, 3rd Edn. McGraw Hill.

RUTLAND, D. F. & JAMESON, G. J. 1970 Theoretical prediction of the sizes of drops in the breakup of capillary jets. *Chem. Engng Sci.* **25**, 1689.

SANZ, A. & MASSEGUER, J. 1985 One-dimensional linear analysis of the compound jet. *J. Fluid Mech.* **159**, 55–68.

SHEN, J. & LI, X. 1996 Instability of an annular viscous liquid jet. *Acta Mech.* **114**, 167–183.

SHKADOV, V. Y. & SISOEV, G. M. 1996 Instability of a two layer capillary jet. *Intl J. Multiphase Flow* **22**, 363–377.

SWEET, R. G. 1964 High frequency oscillography with electrostatically deflected ink jets. *Stanford Univ. Tech. Rep.* 1722.

TAUB, H. H. 1976 Investigation of nonlinear waves on liquid jets. *Phys. Fluids* **19**, 1124–1129.

TOMOTIKA, S. 1935 On the instability of a cylindrical thread of a viscous liquid surrounded by another viscous liquid. *Proc. R. Soc. Lond.* A **150**, 322–337.

VIHINEN, I., HONOHAN, A. & LIN, S. P. 1997 Image of absolute instability in a liquid jet. *Phys. Fluids* **9**, 3117–3119.

YARIN, A. L. 1993 *Free Liquid Jets and Films: Hydrodynamics and Rheology*. Longman.